JOURNAL OF THE KOREAN ASTRONOMICAL SOCIETY
41: 23 ~ 37, 2008 April

CHEMICAL ABUNDANCES OF THE SYMBIOTIC NOVA AG PEGASI

HYOUK KIM[1] AND SIEK HYUNG[2]
[1] Jodrell Bank Observatory, Macclesfield, Cheshire SK11 9DL, UK
E-mail: hkim@jb.man.ac.uk
[2] School of Science Education (Astronomy), Chungbuk National University, Chungbuk 361-763, Korea
E-mail: hyung@chungbuk.ac.kr
(Received February 29, 2008; Accepted April 10, 2008)

ABSTRACT

The high-resolution optical region spectroscopic data of the symbiotic nova AG Peg secured with the Hamilton Echelle Spectrograph at the Lick Observatory, have been analyzed along with the *International Ultraviolet Explorer* UV archive data. We measure about 700 line intensities in the wavelengths of 3859 to 9230Å and identify about 300 lines. We construct pure photoionization models that represent the observed lines and the physical condition for this symbiotic nova. The spectral energy distribution of the ionizing radiation is adopted from stellar model atmospheres. Based on photoionization models, we derive the elemental abundances; C & N appear to be similar to be smaller than the Galactic planetary nebular value while O is enhanced. Our result is compared with the Contini (1997, 2003) who analyzed the UV region spectral data with the shock + ionization model. The Fe abundance appears to be enhanced than that of normal planetary nebulae, which suggests that AG Peg may have formed in the Galactic disk. The models indicate that the temperature of the central star which excite the shell gas may have fluctuated to an unexpected extent during the years 1998 - 2002.

Key words : binaries: symbiotics: interstellar matter: individual(AG Peg), abundances

I. INTRODUCTION

AG Peg (HD 207 757; BD+11°4673) is one of the oldest symbiotic novae, which consists of a hot compact star and a normal M3 giant embedded in a dense ionized nebula. AG Peg underwent a single outburst at least 150 years ago, sometime between 1841 and 1855 (Lundmark 1921; Boyarchuk 1967). After reaching its maximum of about 6^m around the year 1885, its luminosity had gradually decreased and now it is about 9^m, prior to the outburst state. The luminosity of the white dwarf (WD) decreased by a factor of ~ 4 during 1984-1997 (Kenyon et al. 2001). This luminosity decline had been interpreted either as the WD's radius decrease by a factor of ~ 2 under constant temperature (Altamore & Cassatella 1997) or as its temperature increase and an even larger decrease in radius (Schmutz 1996). Our concern is whether the decline of the UV flux in AG Peg during the 1980s is a natural evolutionary stage of symbiotic novae or not. Other well-known symbiotic stars V1016 Cyg and RR Tel also erupted in 1964 and 1944, respectively. These symbiotic stars might eventually undergo a similar spectrum evolution in the future (Eriksson et al. 2006). Therefore a continuous observation and monitoring of the AG Peg spectrum can give us insight into the fate of symbiotic nova at the end of its eruptions.

International Ultraviolet Explorer(*IUE*) observations of AG Peg are available, at both low and high resolution. A comprehensive report on AG Peg and a large set of observations at different orbital phases had been published, e.g. by Kenyon et al. (1993). Furthermore to determine the properties of the central star and the nebular emission, numerous studies of the UV spectra had been carried out based on *IUE* data (Penston & Allen 1985; Mürset et al. 1991; Vogel & Nussbaumer 1994; Nussbaumer et al. 1995; Eriksson et al. 2004; Eriksson et al. 2005; Eriksson et al. 2006), which gave complicated characteristics of the nebular region.

The optical spectra data were less abundant than those of the UV region, although some studies, e.g. Hutchings et al. (1975), were done based on low resolution data. Contini (1997) calculated a composite model (shock + photoionization) for *IUE* UV spectra assuming two–three different regions in the nebula of AG Peg binary system: the narrow-line-emitting nebula and the broad-line-emitting nebula. Later, he argued that at least three nebula regions would be responsible for the UV and optical spectra (Contini 2003). Eriksson et al. (2004) suggested that the UV line spectrum of AG Peg might consist of four different regions: the WD wind, the ionized part of the red giant atmosphere, the wind collision region, and the common envelope. Using intermediate resolution optical spectra along with the visual data of Tomov & Tomava (1992), Tomov (1998) investigated a dynamical change of the nebular environment. This result implied a decreasing mass-loss rate from a hot component as the luminosity of a hot

Corresponding Author: S. Hyung

component decreases.

AG Peg may give a unique opportunity to observe the interaction and dynamic process between two components in a symbiotic binary system – from a scenario of colliding wind to accretion process from a stellar wind. Such a transition which has never been observed, might be observed in this system in near future (see Zamanov & Tomov 1995). Because AG Peg system is perhaps at a transilient dynamic stage, the optical spectroscopic data would be helpful in establishing the time series change or an evolutionary scenario. We investigate the optical spectra using a photoionization model. We assume that the majority of emission is from a limited spherical region surrounding the WD.

In §2, the observations of AG Peg are summarized. In §3, the high dispersion Hamilton Echelle Spectrograph (HES) data and the result of optical line identification are described. In §3, we present theoretical models to predict the emission line flux of optical spectra and the *IUE* UV spectra. As a result, we derive abundance of AG Peg nebula, which are compared with the result by Contini (1997). In §4, we give a brief conclusion for our study.

II. OBSERVATIONS AND DATA REDUCTION

The optical data were all obtained with the HES at the Coudé focus of the 3m Shane Telescope of the Lick Observatory on 1998 September 17, 2001 August 30, and 2002 August 11 respectively. We obtained long and short exposures, i.e. 30 & 10, 30 & 3, and 60 & 5 minutes in years 1998, 2001, and 2002, respectively. See Table 1. The typical seeing was less than $\sim 1''.5$, $\sim 1''.0$, and $\sim 0''.8$ respectively. We used a large 2048 × 2048 pixel CCD, which covered the whole HES echelle pattern at a single exposure. The spectroscopic slit employed was $640\mu m$ in width, which amounted to $\sim 1''.4$ on image size at the Hamilton Telescope Coudé focus. For this slit width, the limiting resolution on the CCD chip was about 2 pixels, which amounted to 0.05Å wavelength dispersion at 3600Å and increased to 0.15Å at 8850Å. Note that toward the red wavelengths, where the prismatic dispersion is lower, the spectral strips tend to be jammed closer together. The slit length of $5''$ was chosen to avoid confusion of successive echelle orders.

For spectral calibration, we took exposures of a Th-Ar arc lamp to set the wavelength dispersion scale, exposures of a dome-quartz lamp to fix a flat field that allowed us to correct for pixel-to-pixel sensitivity fluctuations, and finally, exposures on a standard star of known energy distribution, i.e., BD+28°4211. This standard star was observed with a slightly larger slit size $1''.8 \times 5''$ to eliminate atmospheric dispersion effects served as spectrophotometric standards.

For a calculation of orbital phase of AG Peg, we adopted the ephemeris

$$JD_{\mathrm{Max(V)}} = 2\,442\,710.0 + 816.5 \times E \qquad (1)$$

(e.g., Iben & Tutukov 1996). Refer to the AG Peg. model geometry from the earlier literatures, e.g. Fig. 3 of Contini (1997). At an orbital phase $\phi \sim 0.25$ or 0.75, one would be able to observe the spectra from both the hot WD and the M3 giant star since both stars are on the sky plane. This phase corresponds to the year 1998 optical data. One can see the M3 giant in front of the hot WD at $\phi \sim 0.5$, i.e. the 2001 optical data, whereas one can see the hot WD in front of the giant at $\phi \sim$ =0, i.e. the 2002 optical data.

(a) Iue Lines

There are ten *IUE* spectral data files available for the phases, similarly corresponding to our optical data, $\phi = 10.24$ (1998), 11.56 (2001), and 11.98 (2002), respectively. These are listed in Table 2. All these spectra are low dispersion and taken through the large $10'' \times 23''$ oval entrance aperture of the *IUE* cameras. The *IUE* data were reduced with the *IUE* NEWSIPS routine reduction techniques at the Goddard Space Flight Center. Since the apparent size of AG Peg is small, the *IUE*-observed emission with the *IUE* camera aperture comes from the entire symbiotic nebula. In Fig. 1, we plot the *IUE* SWP 42159 spectra with the identifications from 1200 to 1950Å wavelength region. All spectra were smoothed with a three-point running average. There are many strong lines seen in this figure. For example, CIV 1548,51 & CIII]1908,09 are important for the determination of the C abundance, whereas HeII 1640 can be compared with the optical region HeII 4846.

Although the *IUE* data were not secured during the same period while we carried out the HES observation, we will use the similar phase data, i.e. SWP46061 and LWP29383, near the phase $\phi = 0.50$. The measurements are given in Table 3. Successive columns of Table 3 are the observed and laboratory wavelengths, the ion, Seaton's extinction parameter, k_λ, the extinction-corrected intensity and the measured flux in units of 10^{-14}ergs cm^{-2}s^{-1} in the last column. The extinction corrected intensities are done assuming that I(HeII 1640)/I(HeII 4846) = 6.7 ($T_\epsilon \sim 10\,000$ K) for the 2001's I(HeII 4846) = 115.0 and C=0.04. Here, we

TABLE 1.
OBSERVING LOG OF AG PEG

Date(UT)	Exp(m)	phase(ϕ)
1998 Sep. 17	30, 10	10.24
2001 Aug. 30	30, 3	11.56
2002 Aug. 11	60, 5	11.98

TABLE 2.
IUE SPECTRA OF AG PEG

Spectrum	Exp. (s)	Obs. date	Phase
SWP42159	360	2 Aug. 1991	7.06
LWP20933	360	2 Aug. 1991	7.06
SWP48232	300	25 Jul. 1993	7.94
LWP25994	240	25 Jul. 1993	7.94
SWP48714	300	23 Sep. 1993	8.01
LWP26447	150	23 Sep. 1993	8.01
SWP37419	360	21 Oct. 1989	6.26
LWP16594	360	21 Oct. 1989	6.26
SWP46061	300	25 Oct. 1992	7.61
LWP29383	480	12 Oct. 1994	8.49

adopt an extinction coefficient $C = 1.47E(B-V)$ at Hβ from the optical data and then $A_v = 3.1E(B-V)$ = 0.09.

(b) Optical Lines

We used the National Optical Astronomy Observatory IRAF echelle data reduction package to extract nebular spectral lines from raw images, employing Th-Ar maps (Latham & Sternberg 1977; Palmer & Engeleman 1983) to identify lines. The reduction procedures are described in Hyung (1994). Since the HES produces a high-dispersion spectrum, we are able to clearly discern poor lines severely affected by the telluric absorption, etc. Lines affected by "bleeding" from a strong line in a nearby order may be seriously impacted for the case of the long exposures. This difficulty can be overcome by looking at the other short exposure. Several procedures are available for estimating the accuracy of the measurements. By comparing data obtained different nights and with different chip positions, we can assess the effects of the guiding errors, and the response function. On the absolute flux scale F(Hβ)=100, statistics show that lines weaker than F=1.0 will have errors of 15 - 40%; for lines of range 1.0$\leq F \leq$10.0, errors fall in the interval of 7-20%; for stronger lines, we estimate errors of 3-10%. In Fig. 2 we present two reduced spectral scans to show the quality of our HES data.

We present the year 2002's HES results in Table 4. Because of a large quantity of data, we do not present the years 1998 & 2001 data. However, we present the strongly measured line intensities in Table 6. A large number of optical lines are measured. Successive columns give the measured wavelength (corrected for radial velocity), the wavelength of the most probable identification, the element, the multiplet number from Moore's tabulations (1974, 1993), and Seaton's extinction parameter k_λ (1979). We corrected wavelength from a comparison of the observed wavelengths of the strong lines ($I > 1.0$) with the laboratory wavelengths, using the least squares method; the central wavelengths of the emission profile were converted to

TABLE 3.
IUE SPECTRAL LINE INTENSITY

λ(obs)	λ(lab)	Ion	k_λ^a	Int.	Flux
1239.14	1230.0	C IV	1.641	15.8	1.19
	1238.0	N V			
1370.89	1371.0	O V]	1.353	364.4	28.08
1399.94	1394.0	Si IV	1.307	1132.2	87.61
1485.07	1486.0	N IV	1.231	576.8	44.95
1549.26	1550.0	C IV	1.183	931.8	72.93
1577.64			1.166	175.8	13.78
1622.91	1619.0	N V	1.143	338.7	26.61
1641.82	1640.0	He II	1.135	1150.0	90.41
1664.12	1664.0	O III]	1.128	552.3	43.45
1718.17	1719.0	NIV	1.119	244.1	19.22
1751.11	1750.0	N III]	1.120	269.0	21.18
1820.70		Al II	1.143	299.1	23.50
1848.57			1.162	164.1	12.87
1892.49	1892.0	Si III]	1.207	209.0	16.32
1908.70	1908.0	C III]	1.228	288.1	22.46
2239.77	2253.0	He II	1.571	554.0	41.84
2509.02	2511.0	He II	0.958	178.9	14.30
2732.66	2733.0	He II	0.701	183.6	15.02
2783.33	2793.0	Mg II	0.659	315.2	25.89
2975.21	2983.0	N II	0.532	145.6	12.10
3132.30	3133.0	O II	0.454	225.4	18.87
3205.27	3203.0	He II	0.423	295.5	24.81

heliocentric radial velocities, -20.28 & -19.71 km s^{-1}) for 60 & 5 minute exposures, respectively, following the method of Herrick (1935). The sixth column gives the HES intensity on the scale I(4861)=100.0, after correcting interstellar extinction with $C = 0.04$ assuming the extinction law of Seaton (1979). The seventh column presents the observed HES flux on the scale F(4861)=100.0, while the last column lists the formal root mean square (RMS) percent error, as deduced from the internal disagreement of measurements made with different exposures (whenever two measurements are available). We measured flux of 699 emission lines covering wavelengths of 3859 to 9229Å and among them 308 lines were identified lines but others are not identified in this work.

To identify the lines, we also used the compilations of Corliss & Sugar (1979), and the Fe II line lists of Johansson (1977). At longer wavelengths, there was definite evidence of telluric lines and also night-sky emission lines. These were identified, using the recent work of Osterbrock et al. (1996). However, in order to obtain an accurate line list, we realized that a line identification due purely to wavelength coincidence was not sufficient. Thus the list of line identifications was compared with the spectra of other symbiotic stars, most importantly, CH Cyg (Jurdana-Šepič & Kotnik-Karuza 2002) and RR Tel (Crawford et al. 1999; McKenna et al. 1997), since these are expected

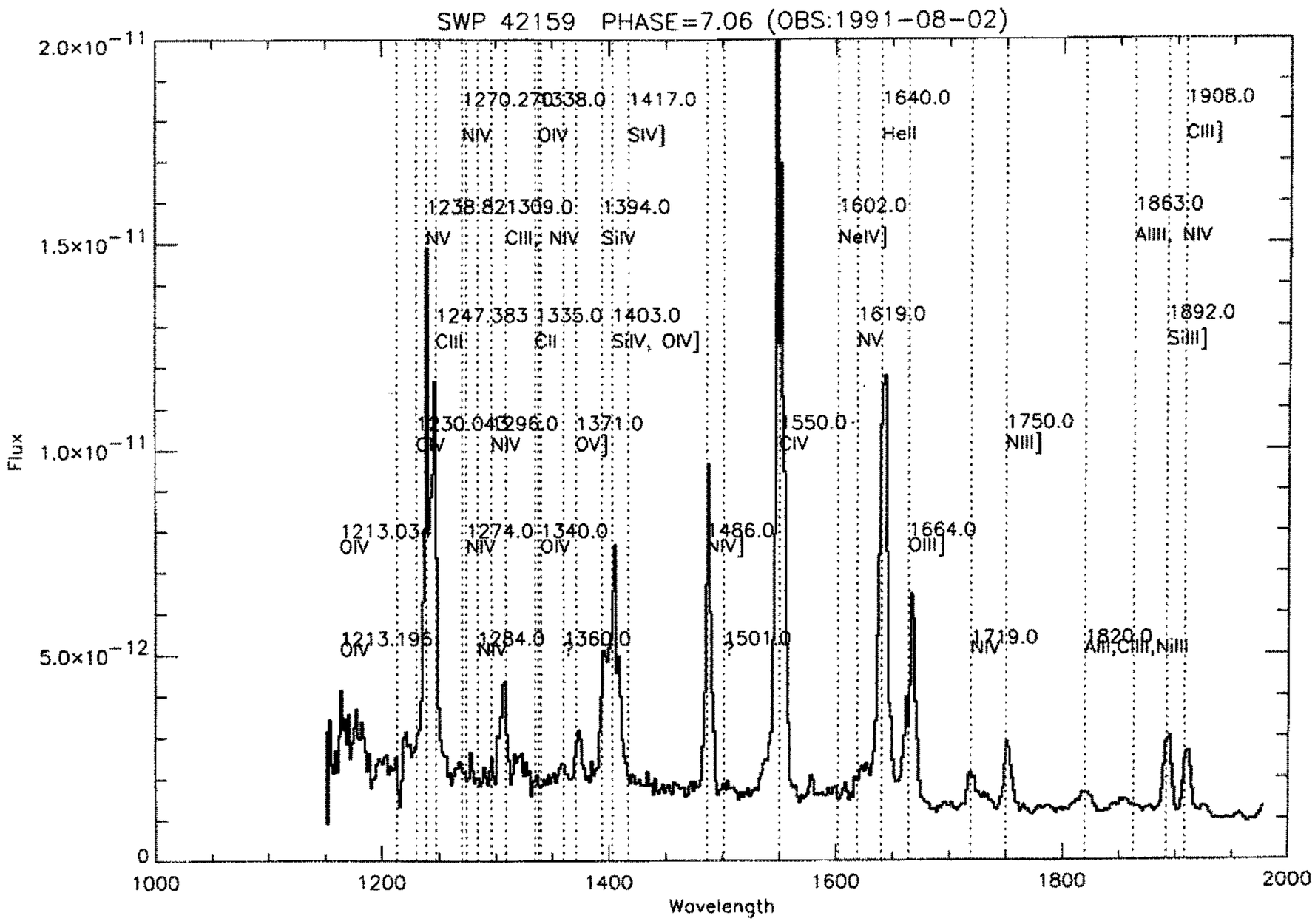

Fig. 1.— UV spectrum of AG Peg (extinction correction not applied in this diagram). Plot was smoothed by a three-point running average.

to have absorption and emission spectra. This proved very useful, as (1) it helped to identify hitherto unknown lines that were not listed in the aforementioned catalogues of line identifications, and (2) when similar lines were present in both spectra, it made the identification of such a line in AG Peg more secure. After these methods were executed, in some cases it was still difficult to decide on a possible identification. Since we have two other spectral data at different phases, it was possible for us to do the work more confidently. With the help of atmospheric model, we were able to fit the background absorption lines. As a result, several iron emissions were clearly identified, i.e., Fe II λ5169.3($3d^54s^2 - 3d^6(^5D)4p$), 5317.0($3d^6(^3G)4s - 3d^6(^5D)4p$), 5363.5, 6443.2($3d^54s^2 - 3d^6(^5D)4p$), and 6457.1($3d^6(^3D)4s - 3d^6(^5D)4p$). Fe II lines might be fluorescence emission lines which are perhaps pumped by UV continuum photons from very low states and decay in optically thin optical lines (see Eriksson et al. 2004). We are not certain at this time that they were produced from PAR (Photoexcitation by Accidental Resonance) processes. These lines and possible pumping mechanism must be carefully investigated in the future study.

We present the observed line intensities of HeI and HeII in Fig. 3. Apparently, the HeI 5876, 6678, & 7065 intensities decrease with time, whereas HeI 4471 does not show such a variation. The high excitation line HeII 4686 intensity is most strongish in 2001 but weakest in 2002. This is probably due to the non-spherical geometry related with the orbital motion of the system. For example, the Hα & Hβ ratio itself shows a variation with phase, indicating that different nebulae contribute to each spectrum (Contini 2003). However, the main cause of the variation is perhaps due to the WD effective temperature fluctuation.

Zamanov & Tomov (1995) predicted that the colliding winds stage would end and the stellar wind would recommence around the year 2001. They expected its gradual decrease and possible minimum luminosity in around the year 2001. Earlier studies evaluated the WD effective temperature based on Zanstra method (HeII 1640 line flux). Their evaluation seems to be too low. Our analysis indicates that the AG Peg WD's temperature fluctuated and it possibly reached the high 150 000 K in the year 2001. See Sec. III.

Numerous lines identified in the present work had been neglected in the earlier studies. In order to ana-

TABLE 4.
OPTICAL SPECTRUM OF AG PEG

λ(obs)	λ(rest)	Element	Mutlitplet	k_λ	Intensity (HES)	Flux (HES)	rms(%)
3859.02	3858.9	[Ni IV]?		0.230	0.065	0.06	
3862.44	3862.59	Si II	(1)	0.230	0.669	0.65	
3867.36		He I?		0.228	0.434	0.42	
3868.79	3868.71	[Ne III]	(1F)	0.228	0.536	0.52	
3871.81	3871.82	He I	(60)	0.227	0.396	0.39	
3882.08	3882.20	O II	(12)	0.225	0.172	0.17	
3886.11		C III?		0.224	0.219	0.21	
3887.31	3887.45	He II		0.223	0.681	0.67	
3888.65	3889.05	H I+He I	H8	0.223	25.288	24.77	17.0%
3891.67	3891.30	[Fe V]?	(3F)	0.222	0.279	0.27	
3895.61	3895.2	[Fe V]		0.221	0.120	0.12	
3900.51				0.220	0.445	0.44	
3905.61	3905.0	[Fe VI]+?		0.219	1.383	1.36	
3911.96	3912.0	O II		0.217	0.017	0.02	
3913.30				0.217	0.256	0.25	
3914.28	3914.5	Fe II		0.216	0.460	0.45	
3918.47	3918.99	C II	(9)	0.215	0.041	0.04	
3918.93	3919.27	O II	(17)	0.215	0.024	0.02	
3920.13	3920.0	O II		0.215	0.032	0.03	
3920.89	3920.68	C II	(4)	0.215	0.009	0.01	
3923.50	3923.45	He II		0.214	0.398	0.39	
3926.51	3926.53	He I	(58)	0.213	0.691	0.68	
3930.35	3930.3	Fe II		0.213	0.327	0.32	
3931.91				0.212	0.097	0.10	
3933.48	3933.7	Ca II?		0.212	1.921	1.88	
3935.79	3935.91	He I	(57)	0.211	0.153	0.15	
3938.13		Fe II		0.211	0.954	0.94	
3945.03	3945.05	O II	(6)	0.209	0.432	0.42	
3953.82	3954.36	O II	(6)	0.207	0.028	0.03	
3958.10	3958.1	[Fe IV]		0.206	0.054	0.05	
3961.45	3961.59	O III	(17)	0.205	0.536	0.53	
3964.59	3964.73	He I	(5)	0.204	2.800	2.75	
3968.23	3968.43	He II	(14)	0.203	2.705	2.65	
3969.91	3970.07	H I	Hϵ	0.203	21.783	21.38	15.0%
3973.01	3973.26	O II	(6)	0.202	0.110	0.11	
3973.48	3973.26	O II	(6)	0.202	0.130	0.13	
3974.02	3973.84	C II	(37)	0.202	0.262	0.26	
3974.61	3974.2	Fe II		0.202	0.022	0.02	
3982.93	3982.72	O II	(6)	0.200	0.020	0.02	
3990.92	3990.3	[Ni IV]?		0.198	0.028	0.03	
3995.11	3995.17	O II	(10)	0.197	0.096	0.09	
3995.82	3995.1	O IV?		0.197	0.023	0.02	
3997.00	3997.29	F IV		0.196	0.184	0.18	
3997.78	3997.29	F IV		0.196	0.169	0.17	
4001.94	4002.1	Fe II		0.195	0.065	0.06	
4003.55	4003.6	[N III]		0.195	0.040	0.04	
4007.19	4007.9	[Fe III]?		0.194	0.031	0.03	
4009.27	4009.27	He I	(55)	0.193	0.986	0.97	
4012.33	4012.7	[Ne III]		0.193	0.307	0.30	
4014.39	4014.6	[Fe VI]		0.192	0.036	0.04	
4018.41	4018.5	Fe II		0.191	0.054	0.05	
4023.86	4023.99	He I	(54)	0.190	0.062	0.06	
4024.35	4024.04	O II	(99)	0.190	0.082	0.08	
4024.97	4025.6	He II		0.190	0.184	0.18	
4025.99	4026.36	He I	(18)	0.190	2.935	2.88	

TABLE 4.
CONTINUED

λ(obs)	λ(rest)	Element	Mutlitplet	k_λ^a	Intensity (HES)	Flux (HES)	rms(%)
4028.18	4028.3	Ti II		0.189	0.178	0.18	
4032.52	4032.48	O II	(51)	0.188	0.010	0.01	
4032.93	4033.16	O II	(51)	0.188	0.038	0.04	
4035.55	4035.1	O II		0.187	0.095	0.09	
4045.65	4046.5	[Fe III]		0.185	0.388	0.38	
4056.02	4056.1	C III		0.183	0.047	0.05	
4057.36	4057.00	N II	(39)	0.182	0.020	0.02	
4060.52	4060.78	O II	(97)	0.181	0.009	0.01	
4068.55	4068.60	[S II]	(1F)	0.180	0.105	0.10	
4069.85	4069.88	O II	(10)	0.179	0.208	0.20	
4071.70	4072.16	O II	(10)	0.179	0.081	0.08	
4072.12	4072.16	O II	(10)	0.179	0.098	0.10	
4075.76	4075.86	O II	(10)	0.178	0.155	0.15	
4076.50	4076.35	[S II]	(1F)	0.178	0.006	0.01	
4078.79	4078.86	O II	(10)	0.177	0.007	0.01	
4083.85	4083.90	O II	(49)	0.176	0.013	0.01	
4084.86	4085.11	O II	(10)	0.176	0.027	0.03	
4087.15	4087.16	O II	(48)	0.175	0.008	0.01	
4088.66	4088.86	O II	(1)	0.175	0.059	0.06	
4089.27	4089.30	O II	(48)	0.175	0.134	0.13	
4093.11	4092.94	O II	(10)	0.174	0.103	0.10	
4093.94	4094.14	O II	(10)	0.174	0.016	0.02	
4100.02	4100.04	He II	(4-12)	0.172	0.583	0.57	
4101.74	4101.76	H I	Hδ	0.172	27.982	27.54	7.0%
4103.35	4103.37	N III	(1)	0.172	0.477	0.47	
4105.42	4105.00	O II	(20)	0.171	0.042	0.04	
4106.67	4107.07	O II	(47)	0.171	0.008	0.01	
4106.97	4107.07	O II	(47)	0.171	0.005	0.01	
4107.36	4107.07	O II	(47)	0.171	0.013	0.01	
4110.84	4110.80	O II	(20)	0.170	0.006	0.01	
4114.30	4114.48	[Fe II]?	(23F)	0.169	0.017	0.02	
4115.95	4116.10	Si IV	(1)	0.169	0.007	0.01	
4119.27	4119.22	O II	(20)	0.168	0.101	0.10	
4120.79	4120.81	He I	(16)	0.168	0.961	0.95	
4121.73	4121.46	O II	(19)	0.168	0.015	0.01	
4122.59	4122.5	[K V]+?		0.167	0.274	0.27	
4124.82	4124.8	Fe II		0.167	0.014	0.01	
4128.09	4128.1	Si II		0.166	0.101	0.10	
4128.68	4128.78	[Fe III]+?		0.166	0.111	0.11	
4129.10	4129.32	O II	(19)	0.166	0.011	0.01	
4132.80	4132.80	O II	(19)	0.165	0.043	0.04	
4138.46	4138.4	Fe II		0.164	0.016	0.02	
4140.79	4140.70	O II	(19)	0.163	0.022	0.02	
	4143.77	O II	(106)				
4143.64	4143.76	He I	(53)	0.163	1.912	1.88	
4145.71	4146.00	O II	(106)	0.162	0.020	0.02	
4145.90	4146.00	O II	(106)	0.162	0.015	0.02	
4146.84	4146.7	[Fe II]+S		0.162	0.025	0.02	
4153.48	4153.30	O II	(19)	0.161	0.024	0.02	
4156.78	4156.53	O II	(19)	0.160	0.063	0.06	
4157.48	4157.5	[F II]		0.160	0.027	0.03	
4162.51	4162.80	C III	(21)	0.159	0.025	0.02	
4163.54	4163.30	[K V]	(1F)	0.158	0.212	0.21	
4168.85	4168.97	He I	(52)	0.157	0.111	0.11	
4173.32	4173.5	Fe II		0.156	0.705	0.70	

TABLE 4.
CONTINUED

λ(obs)	λ(rest)	Element	Mutlitplet	k_λ^a	Intensity (HES)	Flux (HES)	rms(%)
4177.04	4177.21	[Fe II]	(21F)	0.156	0.008	0.01	
4177.58	4177.21	[Fe II]	(21F)	0.156	0.212	0.21	
4178.76	4178.9	Fe II+?		0.156	0.787	0.78	
4181.67	4181.3	[Fe V]?		0.155	0.069	0.07	
4185.60	4185.5	O II		0.154	0.046	0.05	
4186.75	4186.90	C III	(18)	0.154	0.006	0.01	
4187.03	4186.90	C III	(18)	0.154	0.008	0.01	
4190.32	4189.79	O II	(36)	0.154	0.018	0.02	
4192.19	4192.1	Ni II		0.153	0.010	0.01	
4195.25	4195.70	N III	(6)	0.153	0.010	0.01	
4195.61	4195.70	N III	(6)	0.153	0.052	0.05	
4196.05	4196.26	O II	(42)	0.153	0.017	0.02	
4199.81	4199.83	He II	(4-11)	0.152	0.931	0.92	
4201.89	4201.2	[Ni II]?		0.152	0.080	0.08	
4209.02	4209.0	Cr II		0.150	0.041	0.04	
4226.75	4227.19	[Fe V]	(2F)	0.147	0.012	0.01	
4227.25	4227.19	[Fe V]	(2F)	0.147	0.131	0.13	
4229.31	4229.27	[Fe V]		0.147	0.012	0.01	
4233.02	4233.2	[Fe II]		0.146	1.499	1.48	
4238.66	4238.7	Cr II		0.145	0.065	0.06	
4244.10	4243.98	[Fe II]	(21F)	0.145	0.334	0.33	
4244.79	4244.8	[Fe II]		0.144	0.032	0.03	
4245.23	4244.0	[Fe II]		0.144	0.016	0.02	
4246.82	4246.8	Sc II		0.144	0.038	0.04	
4258.03	4258.2	Fe II		0.142	0.188	0.19	
4266.86	4267.18	C II	(6)	0.141	0.017	0.02	
4267.24	4267.18	C II	(6)	0.141	0.092	0.09	
4273.23	4273.3	Fe II		0.140	0.110	0.11	
4275.53	4275.52	O II	(67)	0.139	0.041	0.04	
4276.86	4276.71	O II	(67;54)	0.139	0.047	0.05	
4278.05	4277.89	O II	(67)	0.139	0.157	0.16	
4281.86	4282.02	O II	(80)	0.138	0.036	0.04	
4282.41	4282.02	O II	(80)	0.138	0.021	0.02	
	4285.68	O II	(79)				
4285.29	4285.00	S III	(4)	0.138	0.021	0.02	
4287.28	4287.40	[Fe II]	(7F)	0.137	0.116	0.11	
4287.79	4287.40	[Fe II]	(7F)	0.137	0.068	0.07	
4290.12	4290.2	Ti II		0.137	0.283	0.28	
4290.72	4291.25	O II	(55)	0.137	0.005	0.01	
4293.96	4294.1	Ti II; [Ni?]		0.136	0.148	0.15	
4295.29	4294.78	O II	(54)	0.136	0.027	0.03	
4296.42	4296.6	Fe II		0.136	0.407	0.40	
4303.71	4303.82	O II	(53)	0.135	0.006	0.01	
4304.05	4304.08	O II	(53)	0.135	0.024	0.02	
4311.96	4312.11	O II	(80)	0.133	0.035	0.03	
4312.92	4313.44	O II	(80)	0.133	0.184	0.18	
4315.02	4315.39	O II	(65)	0.133	0.034	0.03	
4317.62	4317.70	O II	(53)	0.133	0.008	0.01	
4319.69	4319.63	O II	(2)	0.132	0.008	0.01	
4333.30	4332.76	O II	(65)	0.130	0.020	0.02	
4335.69	4336.9	O II		0.130	0.029	0.03	
4338.69	4338.67	He II	(4-10)	0.129	0.615	0.61	
4340.61	4340.47	H I	Hγ	0.129	47.770	47.21	17.0%
4344.18	4344.0	Mn II ; Ti II		0.128	0.128	0.13	
4345.64	4345.56	O II	(2)	0.128	0.067	0.07	

TABLE 4.
CONTINUED

λ(obs)	λ(rest)	Element	Mutlitplet	k_λ^a	Intensity (HES)	Flux (HES)	rms(%)
4347.02	4347.20	O II	(16)	0.128	0.022	0.02	
4349.40	4349.43	O II	(2)	0.127	0.111	0.11	
4351.71	4351.27	O II	(16)	0.127	0.785	0.78	
4357.08	4357.25	O II	(63)	0.125	0.020	0.02	
4357.56	4357.25	O II	(63)	0.125	0.032	0.03	
4359.19	4359.40	O II	(26)	0.125	0.065	0.06	
4363.28	4363.21	[O III]	(2F)	0.124	0.708	0.70	
4366.71	4366.90	O II	(2)	0.123	0.043	0.04	
4367.53	4368.1	C II;O I		0.122	0.031	0.03	
4369.27	4369.27	O II	(26)	0.122	0.085	0.08	
4370.54	4370.76	Ar II	(39)	0.122	0.020	0.02	
4371.83	4371.61	O II	(76)	0.121	0.032	0.03	
4376.09	4375.99	O II	(67)	0.120	0.153	0.15	
4378.93	4379.11	N III		0.119	0.109	0.11	
4384.30	4384.3	Fe II		0.118	0.113	0.11	
4385.34	4385.4	Fe II		0.118	0.289	0.29	
4387.87	4387.93	He I	(51)	0.117	3.197	3.16	6.0%
4394.90	4395.0	Ti II		0.115	0.060	0.06	
4395.70	4395.94	O II	(26)	0.115	0.072	0.07	
4399.65	4399.8	Ti II		0.114	0.192	0.19	
4412.88	4413.6	Fe II		0.110	0.026	0.03	
4413.61	4413.78	[Fe II]	(7F)	0.110	0.061	0.06	
4415.10	4414.91	O II	(5)	0.110	0.009	0.01	
4416.21	4416.27	[Fe II]	(3F)	0.109	0.044	0.04	
4416.85	4416.98	O II	(5)	0.109	0.270	0.27	
4426.29	4426.3	[Fe V]		0.107	0.012	0.01	
4428.71	4428.54	Ne II?	(56;61)	0.106	0.017	0.02	
4437.36	4437.55	He I	(50)	0.104	0.231	0.23	
4443.94	4443.8	Ti II		0.102	0.220	0.22	
4446.15	4446.3	Fe II+[Ni?]		0.101	0.029	0.03	
4447.79	4448.21	O II		0.101	0.037	0.04	
4448.58	4448.21	O II		0.101	0.096	0.10	
4450.51	4450.5	Ti II		0.100	0.095	0.09	
4452.33	4452.38	O II	(5)	0.100	0.043	0.04	
4454.00	4454.8	Zr II		0.099	0.031	0.03	
4461.51	4461.4	Fe II		0.097	0.064	0.06	
4468.33	4467.88	O II	(94)	0.096	0.061	0.06	
4468.98	4469.32	O II	(59;94)	0.096	0.022	0.02	
4471.48	4471.48	He I	(14)	0.095	4.053	4.02	
4473.28	4472.9	Fe II		0.094	0.047	0.05	
4477.74	4477.88	O II	(88)	0.093	0.050	0.05	
4478.17	4477.88	O II	(88)	0.093	0.022	0.02	
4479.04	4479.1	[Fe II]		0.093	0.058	0.06	
4482.31	4481.1	Mg II		0.092	0.024	0.02	
4488.54	4488.15	N II	(21)	0.090	0.009	0.01	
4489.15	4489.46	O II	(87)	0.090	0.208	0.21	
4491.31	4491.25	O II	(86)	0.090	0.324	0.32	
4501.12	4501.3	Ti II		0.087	0.138	0.14	
4508.21	4508.3	Fe II		0.085	0.326	0.32	
4510.58	4510.92	N III	(3)	0.085	0.035	0.03	
	4510.93	[K IV]					
4510.91	4510.92	N III	(3)	0.085	0.029	0.03	
4515.35	4514.89	N III	(3)	0.084	0.529	0.52	
4520.28	4520.2	Fe II		0.082	0.374	0.37	
4522.62	4522.6	Fe II		0.082	0.328	0.33	

TABLE 4.
CONTINUED

λ(obs)	λ(rest)	Element	Mutlitplet	k_λ^a	Intensity (HES)	Flux (HES)	rms(%)
4533.96	4534.17	Fe II+Ti?		0.079	0.126	0.12	
4541.55	4541.59	He II	(9)	0.077	1.306	1.30	
4549.46	4549.5	Fe II		0.075	0.869	0.86	
4555.95	4555.9	Fe II		0.073	0.486	0.48	
4558.69	4558.7	Cr II		0.073	0.050	0.05	
4570.98	4571.00	Mg I]	(1)	0.070	0.186	0.18	
4576.19	4576.3	Fe II		0.068	0.189	0.19	
4582.76	4582.8	Fe II		0.067	0.111	0.11	
4583.78	4583.8	Fe II		0.067	1.166	1.16	
4608.34	4607.2	N II		0.061	0.043	0.04	
4610.42	4610.20	O II	(92)	0.060	0.050	0.05	
4620.47	4619.98	N V	(1)	0.058	0.127	0.13	
4629.41	4629.3	Fe II		0.055	0.811	0.81	
4634.20	4634.16	N III	(2)	0.054	0.824	0.82	
4640.57	4640.64	N III	(2)	0.053	1.803	1.79	
4641.83	4641.81	N III	(2)	0.053	0.151	0.15	
4647.22	4647.40	C III	(1)	0.051	0.121	0.12	
4649.06	4649.14	O II	(1)	0.051	0.128	0.13	
4650.27	4650.16	C III	(1)	0.050	0.063	0.06	
4661.71	4661.63	O II	(1)	0.048	0.008	0.01	
4666.85	4667.20	N II	(1)	0.047	0.119	0.12	
4685.71	4685.68	He II	(3-4)	0.042	37.212	37.07	2.0%
4711.10	4711.34	[Ar IV]	(1F)	0.036	0.044	0.04	
4713.17	4713.14	He I	(12)	0.036	2.707	2.70	
4725.51	4725.62	[Ne IV]	(1F)	0.033	0.035	0.04	
4731.37	4731.4	Fe II		0.031	0.118	0.12	
4861.49	4861.33	H I	Hβ	0.000	100.000	100.00	1.0%
4921.84	4921.93	He I	(48)	-0.014	8.579	8.59	6.0%
4923.79	4923.9	Fe II		-0.015	1.508	1.51	
5015.56	5015.68	He I	(4)	-0.036	5.855	5.87	16.0%
5018.35				-0.037	3.066	3.08	
5041.14	5041.06	Si II	(5)	-0.041	0.277	0.28	
5047.67	5047.74	He I	(47)	-0.043	1.553	1.56	
5055.96	5056.02	Si II	(5)	-0.045	0.255	0.26	
5169.14	5168.9	Fe I		-0.068	1.634	1.64	
5197.39	5197.90	[N I]	(1F)	-0.074	1.143	1.15	
5276.15		O I?		-0.090	0.921	0.93	
5316.84				-0.098	2.138	2.16	
5412.16	5412.00	[Fe III]	(1F)	-0.118	3.726	3.77	
5425.32	5424.2	[Fe VI]		-0.121	0.318	0.32	
5534.73	5534.9	[Fe II]		-0.143	0.645	0.65	
5577.75	5577.34	[O I]	(3F)	-0.152	0.253	0.26	
5619.00	5618.7	[Cr II]		-0.161	0.232	0.24	
5721.76	5722.6	Fe II+[Fe?]		-0.184	2.161	2.20	
5875.79	5875.67	He I	(11)	-0.216	19.470	19.86	13.0%
5991.44	5991.4	Fe II		-0.236	0.594	0.61	
6086.69	6086.90	[CaV+Fe?		-0.252	5.740	5.87	
6106.94				-0.255	1.199	1.23	
6300.35	6300.30	[O I]	(1F)	-0.285	0.555	0.57	
6347.01	6347.09	Si II	(2)	-0.292	0.243	0.25	
6371.39	6371.36	Si II	(2)	-0.295	0.233	0.24	
6562.79	6562.82	H I	Hα	-0.323	429.625	442.59	
6678.66	6678.15	He I	(46)	-0.338	20.963	21.63	25.0%
7065.17	7065.28	He I	(10)	-0.383	19.306	20.00	18.0%
7282.00	7281.4	He I		-0.406	5.044	5.24	

TABLE 4.
CONTINUED

λ(obs)	λ(rest)	Element	Mutlitplet	k_λ^a	Intensity (HES)	Flux (HES)	rms(%)
8237.38	8236.8	He II		-0.492	0.799	0.84	
8342.24	8342.20	He I	(4/12)	-0.501	0.365	0.38	
8359.92	8359.66	He I		-0.504	0.237	0.25	
8392.82	8392.40	H I	P20	-0.509	0.353	0.37	
8446.63	8446.48	O I	(4)	-0.517	13.071	13.71	
8490.33	8488.8	He I		-0.524	0.256	0.27	
8498.05	8498.0	Ca II		-0.525	2.553	2.68	
8501.09	8500.2	[Cl III]?		-0.526	0.079	0.08	
	8542.10	Ca II					
8541.70	8541.80	He II	(6-30)	-0.532	5.161	5.42	
8545.48	8545.38	H I	P15	-0.532	0.364	0.38	
	8662.10	Ca II					
8661.71	8662.00	He I	(10/14)	-0.549	4.386	4.61	
8665.29	8665.02	H I	P13	-0.550	0.306	0.32	
8926.33	8925.7	N V		-0.587	0.645	0.68	
9229.06	9229.02	H I	P9	-0.612	1.131	1.20	

The data are from the year 2002 observation. The year 1998 & 2001 optical data are not given, here. See text.

lyze them more fully, one must investigate both their radial velocities and their intensity variation, which is beyond the present study limit.

III. THEORETICAL MODEL AND ABUNDANCE DETERMINATION

The CLOUDY photoionization code by Ferland (1996) was used to fit the spectra of AG Peg nova. We tested various models with different densities as high as 10^{10} cm^{-3}, employing different stellar temperatures for the ionizing hot UV source, e.g. WD or accretion disk. Here, we do not consider a shock heating due to an interacting wind. We assume a different central star temperature for each observation while the nebular shell scale or physical condition remain the same during our observation period. Our models assume a simple spherically symmetric geometry of the nebula gas around a hot WD or a hot accretion disk instead. Hubeny's (1980) model atmosphere was used to generate spectral energy distribution (SED) for a central star temperature, T_{eff} and a surface gravity, log g. The nebular gas may originate not only from the hot component itself, but also from the giant star. However, the current modelling approach assumes that most gas is from the WD. The distance to AG Peg is assumed to be 1000 pc.

Table 5 gives the input parameters adopted in 5 models, i.e. M98 & R98 for 1998, R01 for 2001, and R02 & A02 for 2002. Models, M98, R98, R01, & R02, assume a WD as a hot UV source, whereas the Model A02 adopts an accretion disk SED as a hot UV source. The hot companion temperature of AG Peg was derived as 42 000 - 96 000 K by Altamore & Cassatella (1997); 87 000K by Kenyon et al. (1993); and 95 000 - 10 000 K by Mürset et al. (1991), respectively. After a number of trials, we realized that our pure photoionization model would not give a satisfactory fit to the HeI lines, especially λ5876, 6678, & 7065, using such an information. Thus, we used a little higher temperatures and tried to get the appropriate HeI 4471 & HeII 4686 value and other lines.

We fixed the stellar luminosity and inner radius of the shell. The hot component luminosity was assumed to be 300 $L_\odot$ (see Zamanov & Tomov 1995). The inner boundary of the nebular shell, a distance from the hot star, was assumed to be 3.16×10^8 km, i.e. $\sim$2 AU. This is a bit smaller than the assumed scale by other previous investigation, e.g. r $\sim 2.5\times10^9$ km by Contini (1997). The difference comes from the adopted distance to AG Peg and the inclusion of the shock excitation in the outer region of the system. The outer shell radius in M98 is material bounded, i.e. truncated, whereas all the other models assume a radiation bounded boundary (i.e. Strömgren sphere). The absolute Hβ flux from the nebular gas is about $10^{33.94-33.95}$ erg/s/Å for the radiation bounded ones, at a distance 1000 pc. For the year 1998 data, radiation bounded model did not give a proper prediction on He lines even with a lower WD component temperature, so we truncated the outer radius at 3.178×10^{13} cm or 0.0000103pc.

The adopted hydrogen number densities in models are $10^{9.85}$ and $10^{9.87}$ cm^{-3}. This or a slightly higher value would be suitable to fit the observed [OIII] line intensities: if we lower the number density value, the predicted intensities will be too much strong. The predicted electron temperatures of the nebular gas are

TABLE 5.
INPUT PARAMETERS IN AG PEG MODELS

Parameter	M98[R98]	R01	R02[A02]
Hot star lumi. ($L_\odot$)	300	300	300
Hot star temp. (K)	120 000	150 000	107 000
Gravity (log g, cgs)	6.0	6.0	5.5 [–]
Density (log N_H cm^{-3})	9.85	9.85	9.85[9.87]
Outer radius (cm)	3.178(13) [3.196(13)]	3.208(13)	3.195(13) [3.193(13)]
Electron Temp. (K)	19 500[13 050]	11 000	13 200 [8860]
Abundances	He= 0.126; C= 1.0(-4); Si= 2.5(-5); S= 1.0(-4);	N= 1.3(-6); O= 1.0(-3); Ca=1.0(-5); Fe= 6.3(-4);	Ne= 1.6(-4); Ar= 1.0(-5)

The distance is assumed to be 1000 pc. The inner radius is $10^{13.5}$(i.e. 3.16×10^{13}) cm or about 2 AU in all models. The shell is very thin, so the dimension of the shells is about 4 AU. Abundances are given relative to H. All the abundances are identical in all models, except for He/H = 0.14 in R01. Effective temperature in A02: 100 000 K. $X(-Y)$ implies $X \times 10^{-Y}$.

slightly different. The average electron temperatures are 11 000 – 13 200 K for the radiation bound model, whereas the other models give very different temperatures (see Table 5). Except for He in R01 where He/H = 0.14 assumed, the same abundances are used in all the models.

In Table 6 we compare the predicted intensities along with the observed ones. Columns (1) & (2) give the ion and wavelength responsible for line emission; columns (3), (4), & (5) observed line intensities in 1998, 2001, & 2002, respectively; and columns (6), (7), & (8) predictions, from models M98 & R98, R01, and R02 & A02, respectively. The *IUE* data are given in column (4).

For the extremely strong HeII line of the year 2001, 150 000 K effective temperature seems to be necessary, while for the weakest HeII of the year 2002, about 107 000 K effective temperature seems to be fine. For the year 1998 data, we employed the 120 000 K SED to fit the HeII line. This, however, does not give a satisfactory fit to the HeI 4471. Hence, we check the prediction from the material bounded, as mentioned before. For the 1998 data, the material bounded model M98 prediction gives a slightly better prediction over the radiation bounded model R98. This material bounded or truncated model gives a slightly better fit to the observed HeI 4471 line intensities. We also check the disk SED model for the 2002 data to see if one can improve the prediction. Model A02 was made with the effective disk temperature of 100 000 K. This does not seem to give an improved prediction, though. For the year 2001 data, we only give the prediction from a radiation bounded model R01.

All of our photoionizing models predict the HeI 6678 & 7065, very weakly. Emissions such as HeI singlet at λ 6678Åand metal monovalent ions as OII & NII were found to act in an unforeseen manner to be very weak, while HeI triplet and [OIII] forbidden line correlated relatively well with the current pure photoionization model. The strange behavior of the former lines, i.e., deviation from theory, may be attributed to 2 separate factors. The first is that M II (monovalent ion) like O II and nebular lines emitted in different region, which was supported by work of Hutchings et al. (1975). He had suggested that OII emitted in around M giant and [OIII] near WD. Alternatively, it may be attributed to the other mechanism, i.e. shock heating for HeI lines (see Contini 1997) and fluorescence for OII & NII. Although these lines behaved strangely, their intensities appear to decrease with time.

HeII 4686 intensities as in Fig. 3 seem to give a hint of excitation variation, although the HeI lines do not behave accordingly. The HeII 4686 & HeI 4471 ratios were obtained to see if their values varied according to the excitation of the ionized gas. The observed and predicted $\lambda4686/\lambda4471$ ratios are compared in the last row of Table 6. The predicted ratios seems to agree with the observed ones. The year 2001's HeII 4686 excitation is the strongest; the year 1998 one is the middle; and the 2002 one is the lowest. The gradual decrease of HeI line intensities cannot be accommodated by the current models. Such a variation is perhaps due to the decrease of shock region due to the orbital phase. As mentioned by Contini (1997), the photoionized emission is limited by the viewing angle from Earth. Hence, such a viewing angle and the geometrical effect must be also involved. See Contini (2003).

The nebular region itself may consist of incoherent regions involved with two major excitation mechanisms, i.e. a WD photoionization and a collisional shock heating. The latter contribution to the HeI emissions appear to be large. Apparently, their influence had been gradually decreasing during our observation period. There are other lines, e.g. [NeIV] 4725 & [ArIV] 4711, which were not fitted with our photoion-

TABLE 6.
COMPARISON OF PREDICTIONS WITH OBSERVATIONS

Ion	λ(Å)	1998	2001	2002	M98[R98]	R01	R02[A02]
He I	4471	2.89	3.05	4.05	2.87[3.51]	3.31	4.41[4.46]
	5876	22.61	19.07	19.47	15.33[17.61]	16.75	21.01[21.24]
	6678	34.63	23.80	20.96	2.18[2.68]	2.53	3.39[3.43]
	7065	31.24	23.10	19.31	11.60[13.59]	12.61	14.59[14.87]
He II	4686	77.39	115.0	37.21	82.66[78.16]	102.6	64.16[62.09]
C III]	1908/09		193.9		225.7[116.2]	147.9	215.7[206.7]
C IV	1548/51		627.1		548.4[519.1]	730.7	650.1[621.6]
N III	4640	4.79	4.23	1.80	0.15[0.14]	0.31	0.10[0.10]
N III]	1750		181.0		94.66[95.37]	126.8	173.0[165.1]
N IV	1486		338.2		330.4[313.3]	373.2	233.6[225.6]
[O I]	6300	0.	0.55	0.56	0.0[0.0]	0.0	0.11[0.0]
O II	4102	1.26	3.06	0.45	31.64[32.75]	32.73	33.72[33.64]
[O III]	4363	1.09	2.26	0.71	1.88[1.88]	2.00	2.42[2.37]
O III	1665		371.7		497.4[489.9]	583.2	649.4[626.9]
[S II]	4076	0.61	0.61	0.01	0.0[0.16]	0.17	0.21[0.19]
[S II]	4069	-	0.63	0.10	0.0[0.14]	0.14	0.17[0.16]
Si III]	1892		140.60		209.4[214.7]	204.9	381.7[382.2]
Ca II	3933		0.40		0.15[0.21]	0.28	0.51[0.50]
	3934		0.40		0.10[0.14]	0.18	0.34[0.33]
[Ne III]	3869		1.07		0.74[0.77]	0.69	0.96[0.96]
	3968		0.93		0.22[0.23]	0.21	0.29[0.29]
[Fe V]	3892		0.73		0.75[0.71]	0.73	1.42[0.75]
[Fe VII]	5722	5.52	5.63	2.16	2.83[2.67]	0.32	1.12[1.00]
He*	II /I	26.8	37.7	9.19	28.8[22.3]	31.0	14.5[13.9]

* the line ratios from the relatively close two HeII λ4686 & HeI λ4471, are compared to see the excitation variation.

ization models. Since these collisional lines cannot be produced in such a high density region assumed in our investigation, one must employ a density composite model geometry of having high and low densities in the nebular shell.

Based on our models, we give the recommended abundance of the symbiotic nova AG Peg in Table 7. O & Si abundances are slightly different from those given in Table 5. The previous derivation by Contini (1997) and average planetary nebular abundance are also given in columns (3) & (4). O, Ne, Mg, & Si agree with each other within a factor of 2, while C, N, S, & Fe show a large discordance. Note that our derivation of He is larger than the Contini's, whereas the summed C, N, & O abundance is smaller. Especially, Fe abundance differs by an order. Our Fe abundance which is based on forbidden lines may be in error. Other permitted FeII lines were studied based on the fluorescence mechanism by Eriksson et al. (2004). In order to match ours with such a study, we need to employ a low density region, which has not been done.

Our abundance derivation has been based on the prediction for the optical lines such as HeI 4471Å, HeII 4686Å, [OIII] 4363Å, [SII] 4076Å, [NeIII] 3869Å, [Fe-VII] 3760Åassuming that they are emitted near the hot WD star, whereas Contini (1997, 2003) used the *IUE* data and considered the whole system. Since we do not employ such a sophisticated composite model for the whole system by Contini (1997, 2003) who employed the shocked excitation, our derivation may be only applicable to the limited zone around the WD. Our C &

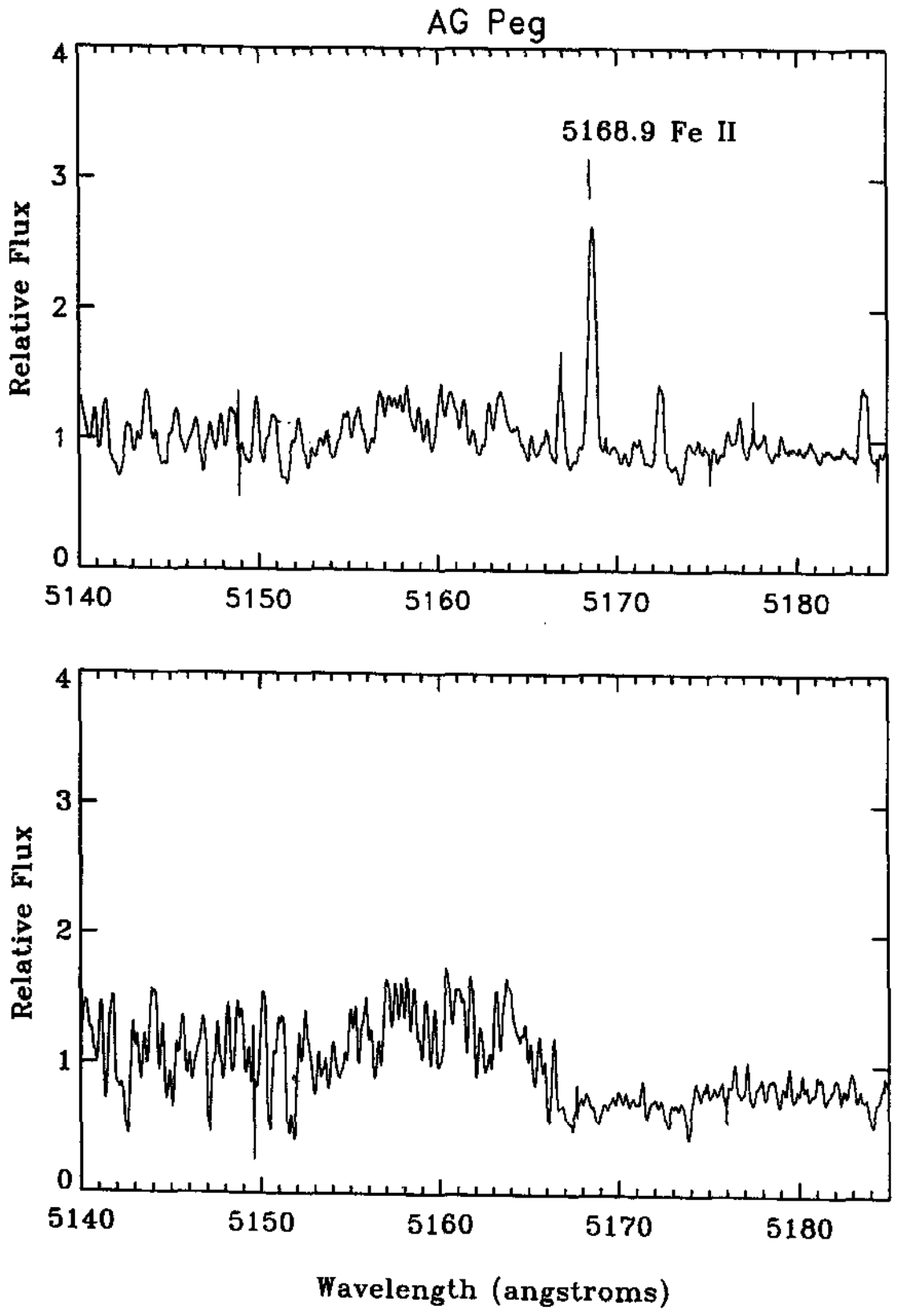

Fig. 2.— Plot of the HES spectrum of AG Peg. Emission lines are dominant in the phase 0.98 spectra shown on the top (2002). The bottom is spectra at phase 0.56 (2001). Radial velocity and interstellar extinction corrections are not applied to these spectral scans.

N abundances are smaller than the galactic planetary nebula value(see Hyung & Feibelman 2004, and reference therein), while O abundance is larger. Our He/H value is on the high side, but He/H=1 used in Contini seems to be too small. We conclude that the abundances by Contini represent the whole system, while ours the zone near the WD.

IV. CONCLUSION

So far, we carried out analysis of the optical spectra of the symbiotic system AG Peg, based on pure photoionization models. With simplified spherically symmetrical geometry, we fitted strategically important optical lines of different orbital phases, near $\phi = 0.0$, 0.25, and 0.5. Our model indicates that the WD effective temperature could be as high as 150 000 K, which are 50 000 K higher than those indicated by other earlier studies. Our models could not fit some of strong lines. Nonetheless, we were able to differentiate lines mainly photoionized by the WD UV radiation from those by other mechanism. The former cases are HeII 4686 & HeI 4471 and other reasonably well fitted cases in Table 6. The model fitting for HeII 4686 and HeI 4471 variation looks fairly fine. Hence, we conclude that the λ4686/λ4471 line ratio had been varied due to the central star temperature fluctuation, although HeI lines might have been affected by other emission mechanism, e.g. shock excitation.

TABLE 7.
RELATIVE ABUNDANCE

Element	AG Peg	C97	PN
He	1.26(−1)	1.0(-1)	0.11
C	1.00(−4)	3.3(−4)	6.48(-4)
N	1.26(−4)	5.3(−4)	1.40(-4)
O	8.00(−4)	9.6(−4)	4.93(-4)
C+N+O	1.03(−3)	1.82(-3)	1.28(-3)
Ne	1.58(−4)	8.3(−5)	1.25(-4)
Mg	3.16(−5)	2.0(−5)	-
Si	2.00(−5)	3.3(−5)	-
S	1.00(−4)	1.6(−5)	8.08(-6)
Ca	1.00(−6)	-	-
Fe	6.30s(−4)	4.0(−5)	

$X(-Y)$ implies $X \times 10^{-Y}$.
C97: from Contini (1997).

In order to fit the rest unpredictable lines, we must try a refinement, tried by various authors, e.g. Contini (1997, 2003). Other alternative would be a density contrast structure geometry in the nebula, i.e. with high density in one direction and low density in the other. We tested a simple density variation in a spherically symmetric geometry, e.g. $N_H \sim N_o/r^2$. This simple structure model did not, however, give any improvement. According to the recent VLA images by Kenny & Taylor (2007), there appears to be a density distribution of enhanced lobe zone and voids exist along the axis, possibly due to the episodic mass loss rate varia-

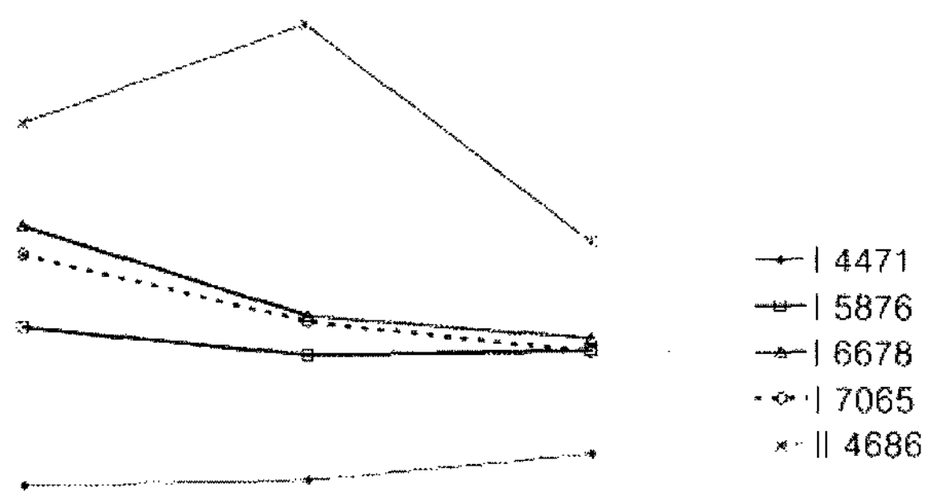

Fig. 3.— He line intensities. The data points are in the order of 1998, 2001 (giant is at the front), and 2002 (WD is at the front). The HeII 4686 and HeI 4471 in Table 4 are rescaled by 1/3 and 3 to show the variation.

tion from the hot component in the earlier evolutionary stage.

Based on the models, we derived the abundances which were compared with those of Contini (1997) and the average PN. Strangely our pure-photoionization based He abundance is so much different from Contini's derivation. More puzzling is that our C, N, & O abundances are smaller than the Contini values. Apparently, He and C, N, & O appear to be anti-correlated in this system. We do not have any proper explanation for this anti-relation at this point. The chemical abundance difference between two approaches might be due to the zonal difference involving the orbital phase change. Geometrical factor and spatial abundance gradient in the system could be also responsible for the difference. Our modelling procedure is a simple approach based on a Cloudy code while Contini's approach is complicated procedure to explain the emission from the whole nebula.

Our C abundance or Contini's value is smaller than the Galactic PN, while O is in an opposite situation, so $O/C \sim 3-8$. The WD of AG Peg appears to be evolved from an O rich progenitor. However, we are not sure of this, since the unknown mass exchange history between two stars and the dredge-up process must be carefully re-examined. Our Fe abundance is also largely different from Contini's value by an order. Our value seems to be overestimated. Our forbidden lines may be emitted from the low density region farther out, while FeII lines must have been produced by fluorescence. Larger Fe/H indicates that AG Peg might be born in the heavily polluted galactic disk region. The WD might be a descendant of about 5 solar mass star on a main sequence phase, which has undergone C fusion reaction during the AGB phase.

In conclusion, our model analysis indicates that the WD temperature varied during our observation period and the shock contribution is perhaps not the primary excitation source of the excitation. The WD temperature might be higher than estimated in the previous literatures. Our identification could be mistaken in some cases. More careful line identification should be done along with an analysis of their radial velocities and many lines which have been classified as unknown in Table 4 must be carefully investigated and identified in the future studies.

ACKNOWLEDGEMENTS

This work was the result of research activities of the Astrophysical Research Center for the Structure and Evolution of the Cosmos (ARCSEC) supported by the Korea Science & Engineering Foundation. S.H. is grateful to the late Prof. Lawrence H. Aller of UCLA, who carried out the Hamilton Echelle observation program, together.

REFERENCES

Altamore, A., & Cassatella, A., 1997, The 1978-1995 variability of the symbiotic star AG Pegasi in the ultraviolet, A&A, 317, 712

Boyarchuk, A. A., 1967, The Nature of AG Pegasi, AZh 44, 12

Contini, M., 1997, The Evolving Structure of AG Pegasi, Emerging from the Interpretation of the Emission Spectra at Different Phases, ApJ, 483, 887

Contini, Marcella, 2003, An analysis of the emission line spectra of AG Pegasi between phases 7.34 and 9.44, MNRAS, 339, 125

Corliss, C., & Sugar, J., 1979, Energy levels of titanium, Tii through Ti xxii, J. Phys. Chem. Ref. Data, 8, 1

Crawford, F. L., McKenna, F. C., Keenan, F. P., Aller, L. H., Feibelman, W. A., & Ryan, S. G., 1999, Line identifications and intensities for the optical spectrum of RR Telescopii between 3180 and 9455Å A&AS, 139, 135

Eriksson, M., Johansson, S., & Wahlgren, G. M., 2004, Modeling the wind structure of AG Peg by fitting of C IV and N V resonance doublets, A&A, 422, 987

Eriksson, M., Johansson, S., & Wahlgren, G. M., 2006, The nature of ultraviolet spectra of AG Pegasi and other symbiotic stars: locations, origins, and excitation mechanisms of emission lines, A&A, 451, 157

Eriksson, M., Johansson, S., Wahlgren, G. M., Veenhuizen, H., Munari, U., & Siviero, A., 2005, Bowen excitation of N III lines in symbiotic stars, A&A, 434, 397

Eriksson, M., Veenhuizen, H., Wahlgren, G. M., & Johansson, S., 2004, Fe II fluorescence in symbiotic stars, RevMexAA, 21, 132

Ferland, G., 1996, in HAZY, Univ. Kentucky Dept. Phys. Astron. Internal Rep.

Herrick, S., 1935, Tables for the reduction of radial velocities to the Sun, Lick Obs. Bull., 17, 85

Hubeny, I., 1988,A computer program for calculating non-LTE model stellar atmospheres, Computer Phys. Comm., 52, 103

Hyung, S., 1994, Density contrast shell models for the planetary nebula IC 2165, ApJS, 90, 119

Hyung, S. & Feibelman, W. A., 2004, Optical and IUE Spectra of the Planetary Nebula NGC 7026, ApJ, 614, 745

Hutchings, J. B., Cowley, A. P., & Redman, R. D., 1975, Mass transfer in the symbiotic binary AG Pegasi., ApJ, 201, 404

Iben, I. J. & Tutokov, A. V., 1996, On the Evolution of Symbiotic Stars and Other Binaries with Accreting Degenerate Dwarfs, ApJS, 105, 145

Johansson, S., 1977, Forbidden Transitions of Fe II., Phys. Scr., 15, 183

Jurdana-Šepič, R., & Kotnik-Karuza, D., 2002, Atlas of M7III Spectral features in the optical (Physics Department, University of Rijeka, Croatia)

Kenny, H. T. & Taylor, A. R., 2007, Colliding Winds in Symbiotic Binary Systems. II. Colliding Winds Geometries and Orbital Motion in the Symbiotic Nova AG Pegasi, ApJ, 662, 1231

Kenyon, S. J., Mikolajewska, J., Mikolajewski,, M., Polidan, R. S., & Slovak, M. H., 1993, Evolution of the symbiotic binary system AG Pegasi - The slowest classical nova eruption ever recorded, AJ, 106, 1573

Kenyon, S. J., Proga, D., & Keyes, C. D., 2001, The Continuing Slow Decline of AG Pegasi, AJ, 122, 349

Latham, D. W. & Sternberg, A., 1977, CfA Preprint 827

Lundmark, K., 1921, Mitteilung uber Nova Cygni 1920, Astron. Nachrichten 213, Nr. 5094, 93

McKenna, F. C., Keenan, F. P., Hambly, N. C., Allende Prieto, C., Rolleston, W. R. J., Aller, L. H., & Feibelman, W. A., 1997, The Optical Spectral Line List of RR Telescopii, ApJS, 109, 225

Moore, C. E., 1974, in Nat. Bur. Standards 40, Multiplet Table of Astrophysical Interest (Princeton: Princeton Univ. Press)

Moore, C. E., 1993, Tables of Spectra of H, C, N, and): Atoms and Ions, ed. J. W. Gallagher (London:CRC)

Mürset, U., Nussbaumer, H., Schmid, H. M., & Vogel, M., 1991, Temperature and luminosity of hot components in symbiotic stars, A&A, 248, 458

Nussbaumer, H., Schmutz, W., & Vogel, M., 1995, Proof of a Fast Wind in the Symbiotic Nova Ag-Pegasi, A&A, 293, L13

Osterbrock, D. E., Fulbright, J. P., Martel, A. R., Keane, M. J., Trager, S. C., & Basri, G., 1996, Night-Sky High-Resolution Spectral Atlas of OH and O2 Emission Lines for Echelle Spectrograph Wavelength Calibration, PASP, 108, 277

Palmer, B. A. & Engeleman, J. R., 1983, Atlas of the Thorium Spectrum (Los Alamos National Laboratory)

Penston, M. V. & Allen, D. A., 1985, On the ultraviolet spectrum of AG Peg, MNRAS, 212, 939

Schmutz, W., 1996, Science with the *HST*-II, ed. F. D. M. Piero Benvenuti, & J. S. Ethan (Baltimore: STScI), 366

Tomov, N. A. & Tomova, M. T., 1992, Radial velocities investigation of symbiotic AG Peg., Izv. Krym. Astrofiz. Obs. 86, 19

Tomov, N. A. & Tomova, M. T., & Raikova, D. V., 1998, The visual line spectrum of AG Pegasi in 1995 A&AS, 129, 479

Vogel, M. & Nussbaumer, H., 1994, The hot wind in the symbiotic nova AG Pegasi, A&A, 284, 145

Zamanov, R. K. & Tomov, N. A., 1995, AG Pegasi: will accretion begin soon?, The Observatory, 115, 185